ECCOMAS Congress 2016
VII European Congress on Computational Methods in Applied Sciences and Engineering
M. Papadrakakis, V. Papadopoulos, G. Stefanou, V. Plevris (Editors)
Crete Island, Greece, 5–10 June 2016

INVESTIGATION OF A MODERN & HYBRID TURBULENCE MODELLING APPROACH FOR TRANSIENT AUTOMOTIVE AERODYNAMICS SIMULATIONS

René Devaradja[1], Petr Šimánek[1], Jacques Papper[1], and Pavla Polická[2]

[1] ICON Technology & Process Consulting SAS
7 rue Auber, 31000 Toulouse, France
e-mail: {r.devaradja,p.simanek,j.papper}@iconcfd.com

[2] ŠKODA AUTO a.s.
tř. Václava Klementa 869, 293 60 Mladá Boleslav, Czech Republic
pavla.policka@skoda-auto.cz

Keywords: Turbulence Modelling, Automotive Aerodynamics, Transient Simulation, PANS, Zeta-f, iconCFD®.

Abstract. *In order to achieve accurate transient predictions of turbulent flow fields on industrial scale problems, it is necessary to use a turbulence model since Direct Numerical Simulation (DNS) would be prohibitively expensive. Unsteady Reynolds-Averaged Navier Stokes (URANS) is the most commonly used to fully model the turbulence as an additional eddy viscosity using the Boussinesq approximation. Large Eddy Simulation (LES) is another modelling approach, which can be more accurate than URANS as only the smallest scales of turbulence are modelled. However, LES mesh requirements are very demanding, and too constraining for simple use in industrial contexts. Therefore, a variety of hybrid models have been developed, attempting to use the provided mesh to its maximum potential by resolving as many turbulent scales as possible and only model those eddies for which the mesh is insufficiently fine. Detached Eddy Simulation (DES), is one example of hybrid model, where URANS is used in the attached boundary layer regions whilst LES is used in the largely separated flow regions where the larger scales are dominant. More recently, the Partially-Averaged Navier Stokes (PANS) method introduced by Girimaji et. Al [3] provides an interesting framework allowing the modification of existing URANS models to resolve the larger scales of turbulence whilst modelling the smaller ones.*

A validation of the PANS zeta-f model using iconCFD® is presented on a variety of cases ranging from cylinder flows to fully detailed vehicle aerodynamics courtesy of ŠKODA AUTO. Comparison to experimental wind-tunnel testing of the Yeti, Fabia and Superb models are presented. Various modifications to the modelled-to-resolved scale ratio are proposed and tested. Successful performance of this model is demonstrated within the industrial context of vehicle aerodynamics, and superiority of this model is shown in the prediction of separation regions, off-body flow structures, and aerodynamic forces.

1. Introduction

Although URANS is generally an attractive turbulence modelling approach for industrial applications owing to its reasonable computational cost, on the other hand its lack of accuracy in the prediction of unsteady bluff body separation flows – which is the main focus of the present paper - raises the need for alternative solution methods. The problematic limitation of URANS resides in its inherent inability to simulate a broad spectrum of turbulent scales since all eddies are modelled. The resulting drawback is a simplified representation of the turbulence physics suffering from a shortfall in large scale characteristics that are influential in the evolution of the turbulent coherent structures. The Large Eddy Simulation (LES) approach is a suitable candidate to overcome this deficiency in accuracy as it directly resolves for the large turbulent scales, dominant in largely separated flows, and also simulates their interaction with the smaller sub-grid scales. This method allows to capture most of the flow details – if not all of them like in Direct Navier Stokes (DNS) - and to represent the overall flow complexity with a satisfactory physical fidelity. However in the near-wall regions, the largest turbulence scales are still very small making the LES approach computationally too expensive. Therefore from an engineering perspective, the LES technique may not be an adequate choice if the turbulent structures of interest are essentially in the outer wall regions, which is typically the case for ground vehicles aerodynamics. Yet, the motivation to apply LES far away from the walls, and to combine it with an affordable but accurate-enough modelling approach valid in the wall vicinity, has led to the development of various and successful hybrid LES/RANS methods as described in [1]. One of the main addressed challenges for these hybrid approaches is the capacity to enable LES in the mesh regions which are fine enough for the local scales to be resolved and bridge it, in a seamless way, with RANS which is invoked in the other regions that do not satisfy the former criterion. In the same spirit of hybrid LES/RANS, a new emerging modelling approach, classified as "second generation URANS", is intended to resolve the energy-containing scales at reduced computational cost. It is called "Partially-Averaged Navier Stokes" (PANS) and was first introduced by Girimaji [2] as a variant of the standard $k-\varepsilon$ closure model. The key feature of this approach is based on the introduction of two new parameters, denoted by f_k and f_ε, which control the relative amount (with respect to the total quantity) of the unresolved turbulent kinetic energy and dissipation rate respectively. Along with appropriate modifications of the closure coefficients, these modelled-to-total scale ratios allow to set the physical resolution of the turbulent fluctuations to any level ranging from pure URANS ($f_{k,\varepsilon}=1$) to pure DNS ($f_{k,\varepsilon}=0$). The mesh resolution to be employed will directly depend on the $f_{k,\varepsilon}$ value if the latter is prescribed as a constant parameter. To remove that dependency, Girimaji [3] suggested a spatially-varying formulation of $f_{k,\varepsilon}$, based upon the local grid dimensions, so that the PANS model can self-adjust its performance to its maximum resolution potential on any grid. In this paper, the PANS $\zeta-f$ model [4] will be retained for further investigations, within the iconCFD® framework, as it should theoretically show a better predictive capability for the near-wall flows in comparison to the original PANS $k-\varepsilon$

formulation. The implementation guidelines of the PANS model, and the different viable options for the $f_{k,\varepsilon}$ computation, are provided and discussed. The model is then evaluated for a set of different bluff body transient flows ranging from the academic square cylinder case to an external aerodynamics simulation on a ŠKODA car model. Finally, the validity of the new eddy-resolving method is assessed through qualitative analysis of turbulent structures and comparison of the numerical results with available experimental data.

2. PANS $\zeta - f$ model description.

2.1. PANS governing equations

The general PANS formulation is derived from the incompressible Navier-Stokes equations by applying an arbitrary filter, denoted by $< \cdots >$, to the instantaneous velocity $\boldsymbol{V}$ and pressure p fields**.** The resulting filtered equations [2] read:

$$\partial_t U_i + U_j \partial_j U_i + \partial_j \tau_{ij} = \frac{1}{\rho} \partial_i p_f + \nu \partial_{jj}^2 U_i$$
$$\partial_{ii}^2 p_f = \partial_j U_i \partial_i U_j + \partial_{jj}^2 \tau_{ij}$$

Where $U_i =< V_i >$ and $p_f =< p >$ are the filtered velocity and pressure fields respectively. The sub-filter scale stress τ_{ij}, assimilated to the Reynolds stress [5], can be calculated using the Boussinesq approximation:

$$\tau_{ij} = -\nu_u S_{ij}$$
$$S_{ij} = \frac{1}{2}\left(\partial_j U_i + \partial_i U_j\right)$$

The unknown variable ν_u, which represents the eddy viscosity of the unresolved scales is then determined by any turbulence closure model. For models of the $k - \epsilon$ family, it is generally expressed as a function of unresolved turbulent kinetic energy k_u and dissipation rate ϵ_u:

$$\nu_u = f(k_u, \epsilon_u)$$

The relation between the unresolved (sub-filtered) and averaged (filtered) turbulence is established in the following way:

$$f_k = \frac{k_u}{k_{tot}} = \frac{k_u}{k_u + 0.5\overline{(\boldsymbol{U} - \overline{\boldsymbol{U}})^2}}$$

$$f_\epsilon = \frac{\epsilon_u}{\epsilon_{tot}} \approx 1$$

The parameters f_k and f_ϵ represent the unresolved-to-total ratios of the turbulent kinetic energy and dissipation rate respectively. Inserting these into any existing URANS closure model allows its adaptation to the PANS framework and controls the level of physical resolution of the turbulence fluctuations ($\boldsymbol{U} - \overline{\boldsymbol{U}}$), with $\overline{\boldsymbol{U}}$ referring to the mean statistical velocity field. A unit value of f_k means that the filtered fluctuations are zero. In other terms, the filtered velocity is equal to its time-averaged value and the PANS model completely switches to the standard URANS formulation. If $f_k = 0$, then $k_u = \nu_u = \tau_{ij} = 0$ and the PANS equations collapse to the DNS ones as the filtered and instantaneous velocities are the same. For intermediate f_k values, the filtered velocity can be called "partially averaged" as the contribution of both resolved and unresolved turbulent fluctuations is non-zero. Finally, the parameter f_ϵ can be set to 1 [3] – at least for high Reynolds number flows - since the very small dissipation scales, which are isolated from the larger energy-containing ones, are not intended to be resolved.

2.2. PANS $\zeta - f$ closure model

Here the $\zeta - f$ model, suggested by Basara [4], is used to close the PANS equations. This model is derived from the URANS $\zeta - f$ model, introduced by Hanjalic [6], and which is known to deal better than its parent, the standard $k - \epsilon$ model, with anisotropic and curvature effects encountered in some wall-bounded turbulent flows. The equations of PANS $\zeta - f$ read:

$$\nu_u = C_\mu \zeta_\mu \frac{{k_u}^2}{\epsilon_u}$$

$$\partial_t k_u + U_j \partial_j k_u = P_u - \epsilon_u + \partial_j \left[\left(\nu + \frac{\nu_u}{\sigma_{ku}} \right) \right] \partial_j k_u$$

$$\partial_t \epsilon_u + U_j \partial_j \epsilon = C_{\epsilon 1} P_u \frac{\epsilon_u}{k_u} - C_{\epsilon 2}^* \frac{\epsilon_u^2}{k_u} + \partial_j \left[\left(\nu + \frac{\nu_u}{\sigma_{\epsilon u}} \right) \partial_j \epsilon_u \right]$$

$$\partial_t \zeta_u + U_j \partial_j \zeta_u = f_u - \frac{\zeta_u}{k_u} \epsilon_u (1 - f_k) + \partial_j \left[\left(\nu + \frac{\nu_u}{\sigma_{\zeta u}} \right) \partial_j \zeta_u \right]$$

$$L_u^2 \nabla^2 \mathrm{f_u} - \mathrm{f_u} = \frac{1}{T_u} \left(C_{f1} + C_{f2} \frac{P_u}{\epsilon_u} \right) \left(\zeta_u - \frac{2}{3} \right)$$

The different terms from the previous equations are: k_u - unresolved turbulent kinetic energy; ϵ_u - dissipation rate of k_u; $P_u = -\tau_{ik}\, \partial_k U_i$ - production rate of k_u; ζ_u - unresolved wall normal velocity scale; f_u - elliptic relaxation function; $L_u = C_L \max \left[\frac{k_u^{1.5}}{\epsilon}, C_\eta \left(\frac{\nu^3}{\epsilon} \right)^{0.25} \right]$ - turbulent length scale; $T_u = \max \left[\frac{k_u}{\epsilon}, C_\tau \left(\frac{\nu}{\epsilon} \right)^{0.5} \right]$ - turbulent time scale. The closure coefficients are given in Table 1.

C_μ	$C_{\epsilon 1}$	$C^*_{\epsilon 2}$	$C_{\epsilon 2}$	C_{f1}	C_{f2}
0.22	$1.4\left(1+\frac{0.045}{\sqrt{\zeta_u}}\right)$	$C_{\epsilon 1}+f_k(C_{\epsilon 2}-C_{\epsilon 1})$	1.9	0.4	0.65
σ_{ku}	$\sigma_{\epsilon u}$	$\sigma_{\zeta u}$	σ_k	σ_ϵ	σ_ζ
$\sigma_k\frac{f_k^2}{f_\epsilon}$	$\sigma_\epsilon\frac{f_k^2}{f_\epsilon}$	$\sigma_\zeta\frac{f_k^2}{f_\epsilon}$	1.0	1.3	1.2
C_L	C_η	C_τ			
0.36	85	6.0			

Table 1 Closure coefficients of PANS $\zeta-f$

If $f_k=1$, then any PANS model should, in theory, be identical to its parent URANS version. Here a few differences can be noted between PANS $\zeta-f$ and URANS $\zeta-f$: (a) in the ϵ transport equation, the isotropic turbulence length scale $\frac{k}{\epsilon}$ is used instead of T; (b) the realizability constraints for T and L are removed; (c) the definition of $C_{\epsilon 1}$ differs from the original URANS one $C_{\epsilon 1}=1.4\left(1+\frac{0.012}{\zeta_u}\right)$.

Finally, the zero transport model [2] is used by Basara to calculate the unresolved turbulent Prandtl numbers ($\sigma_{ku},\sigma_{\epsilon u},\sigma_{\zeta u}$). The maximum transport assumption [2] will be also considered in this paper. According to that model, the following assumptions can be made: $\sigma_{ku}=\sigma_k;\ \sigma_{\epsilon u}=\sigma_\epsilon;\ \sigma_{\zeta u}=\sigma_\zeta$.

2.3. Near-wall treatment

The $\zeta-f$ model is a low Reynolds model which requires, by its nature, a fine wall-normal mesh discretization in order to resolve the whole boundary layer. Thus the required y^+value for such a model is less than 1 to accurately predict the near-wall flow. Because these mesh-related constraints are not easy to satisfy in an industrial context, a hybrid wall treatment which combines the integration to the wall (ITW) with generalised wall functions (GWF), is incorporated into the PANS turbulence model. This method allows to cover all y^+ values, even those falling into the critical buffer region $(5<y^+<30)$. In this study, the compound wall treatment (CWT) approach, proposed by Popovac et al. [7], is adopted to define the wall boundary conditions of the turbulent variables. The general form of CWT, for any flow variable ϕ, is given by:

$$\phi_P=\phi_v e^{-\Gamma}+\phi_t e^{-\frac{1}{\Gamma}}$$

The index "P" denotes the centre of the wall-adjacent cell. The indices "v" and "t" respectively stand for the viscous and turbulent contributions of ϕ. Finally, Γ represents the Kader's blending coefficient. The previous decomposition is applied to the fields $P_u,\epsilon_u,\ f_u$ and ν_u as

reported in Table 2. The different terms involved in the near-wall treatment are: ν_l - the laminar viscosity; y - the wall distance; $y_P^* = \frac{C_{\mu w}^{0.25} k_P^{0.5} y_P}{\nu_l}$; $C_{\mu w} = 0.07$ - the non-dimensional wall distance; $u^* = C_{\mu w}^{0.25} k^{0.5}$ - the turbulent velocity scale; $\kappa = 0.41$ - the Von Karman constant; $u_\tau = \sqrt{(\nu_l + \nu_{u,P})\frac{U_P}{y_P}}$ - the friction velocity; $E = 8.3$ - the log-law constant.

$\boldsymbol{\phi}$	$\boldsymbol{\phi_\nu}$	$\boldsymbol{\phi_t}$	$\boldsymbol{\Gamma}$
ϵ_u	$\frac{2\nu_l k_u}{y_P^2}$	$\frac{u_P^{*3}}{\kappa y_P}$	$0.001\frac{y_P^{*4}}{1+y_P^*}$
P_u	$C_\mu \zeta_{u,P} \frac{k_{u,P}^2}{\epsilon_{u,P}} \left(\frac{U_P}{y_P}\right)^2$	$\frac{u^{*2} u_\tau}{\kappa y_P}$	$0.01\frac{y_P^*}{1+5y_P^*}$
ν_u	ν_l	$\frac{\kappa u_p^* y_P}{\ln(E y_P^*)}$	
f_u	$-\frac{2\nu_l \zeta_P}{y_P^2}$	0	0

Table 2 CWT formulation for PANS $\zeta - f$

2.4. Model implementation

The PANS $\zeta - f$ model along with the enhanced CWT method has been implemented in iconCFD® which is a finite volume CFD code. In this section, the different possible ways of modelling the PANS key parameter f_k are presented and discussed.

The easiest option would be to treat f_k as a user-defined constant coefficient. However this method is impractical for two main reasons. First, in a case where the turbulent flow structures locations are unknown in advance, the engineer will not know where to refine the mesh. Secondly, in some areas of the flow it may be easy to refine the mesh enough to satisfy the prescribed f_k value while in other regions such as boundary layers the required refinement would become prohibitive. Alleviating these constraints, Girmaji [3] suggested another approach by which the f_k variable self-adjusts its value based on the local grid dimensions. This new method, which is more suitable for an industrial process, allows the PANS model to be used at its maximum resolution potential on an arbitrary mesh. The spatially dynamic formulation of f_k is given by:

$$f_{k,min}(x) = \frac{1}{\sqrt{C_\mu}} \left(\frac{\Delta}{\Lambda}\right)^{\frac{2}{3}}$$

The subscript "min" indicates that there is not any strict restriction to apply a larger value than the right-hand term of the above equality. The local grid length scale is denoted by Δ. The variable $\Lambda = \frac{k_{tot}^{1.5}}{\epsilon_u}$ represents the Taylor scale of turbulence.

The only difficulty at this stage is to determine an accurate way to calculate k_{tot} during the PANS simulation. In order to achieve this, it is necessary to know the time-averaged velocity field in advance, or in other terms to estimate that missing field by means of a pre-computed flow solution. Four different methods to estimate k_{tot} are suggested hereafter. For all of them, it is assumed that a converged RANS $\zeta - f$ solution has been obtained beforehand and used for the initialisation of the transient simulation.

Method 1 (GB1) - At each time step n, the value of k_{tot} is updated from the solution at the previous iteration $n-1$, following the definition of f_k:

$$k_{tot}^{n} = \frac{k_u^{n-1}}{f_k^{n-1}}$$

The initial value of f_k is 1.

Method 2 (GB2) – The formula of k_{tot} is simplified by removing the resolved contribution so that at each time step n:

$$k_{tot}^{n} = k_u^{n-1}$$

This simplification is acceptable as it just overestimates the value of f_k^n but the counter-part of this assumption is that some turbulent scales that could have been physically resolved by the grid - with a more correct estimation of f_k^n - will end up being modelled.

Method 3 (GB3) – At each time step n, k_{tot} is estimated from the filtered velocity fluctuations:

$$k_{tot}^{n} = k_u^{n-1} + 0.5(\boldsymbol{U^n} - \overline{\boldsymbol{U}}^n)^2$$

The time-averaged velocity $\overline{\boldsymbol{U}}$ is first initialised with the steady RANS velocity field and then updated in the course of the simulation as $\overline{\boldsymbol{U}}^n$, the running average of $\boldsymbol{U}$.

Method 4 (GB4) – At each time step n, k_{tot} is estimated using the real definition of the resolved turbulent kinetic energy:

$$k_{tot}^{n} = k_u^{n-1} + 0.5\left(\overline{u_i u_i}^{n-1}\right)$$

The time-averaged resolved fluctuations $\overline{u_i u_i}$ are initialised to 0 and then updated in the course of the simulation as $\overline{u_i u_i}^n$, the running average of $u_i u_i$.

After f_k is computed, a few precautions need to be taken with respect to that variable. First, the near-wall cell field should be explicitly set to 1 in case it does not converge to that value. This insures, in the DES spirit, that the turbulent scales in the extreme wall vicinity will be all modelled by URANS. Secondly, the maximum allowed value for f_k must not exceed 1 and its minimum value can be set to any user-defined value (as low as possible) in order to help stabilize the transient solution.

3. PANS Validation

3.1. General Workflow

The numerical simulations are performed with the CFD suite iconCFD®. The computational grids are created with the included automatic unstructured, hex-dominant mesh generator iconHexMesh. The flow is simulated using a two-step process in order to obtain a proper initial estimate of f_k for the PANS calculation. First, a steady flow solution is computed using the RANS $\zeta - f$ model. For this preliminary computation, all the convection terms are approximated by a first-order upwind scheme to ensure solution stability. Once the steady solution is obtained, it is then used for the initialisation of the PANS simulation. For this second calculation phase, a second-order upwind convection scheme is applied to the momentum equation only. The maximum transport model is enabled for the calculation of the turbulent diffusion coefficients. The time step is automatically adjusted by the solver during the transient simulation so that the maximum value of the CFL number does not exceed 1.0.

3.2. Academic Cases

In this section, a primary verification study will be carried out to check the PANS performance in transient bluff-body flows that are commonly used as base benchmarks for LES simulations. In the following sections, the modelled flow is assumed to be incompressible and dependent on the Reynolds number only. The fluid density and kinematic viscosity are arbitrarily set to $1\ kg.m^{-3}$ and $1.5e^{-05}\ m^2.s^{-1}$ respectively. The reference velocity is then deduced from the characteristic length scale of the problem.

3.2.1. Flow past a square cylinder

The different f_k implementations should be initially evaluated in a simple turbulent flow with negligible wall interactions like the one past a square cylinder. The coherent vortical shedding developing in this configuration has been accurately analysed in many research works such as the experimental study conducted by Lyn et al. [8], [9] or the LES simulations performed by Rodi et al. [10]. Reproducing these well-known turbulence characteristics with the PANS model would be a first critical success factor.

Case Description

The Reynolds number for the concerned flow, based on the square cylinder side D, is 21400. This gives a reference bulk velocity of 0.3 $m.s^{-1}$, if D is set to $1m$. The geometric dimensions of the computational domain, are shown in Figure 1. Among the available reference data, those which are retained for comparative analysis are the Strouhal number (Str), the mean drag coefficient (C_D) and the mean stream-wise velocity profile on the centre plane of the cylinder. Further details with respect to the experimental protocol and data can be found on the ERCOFTAC website [12].

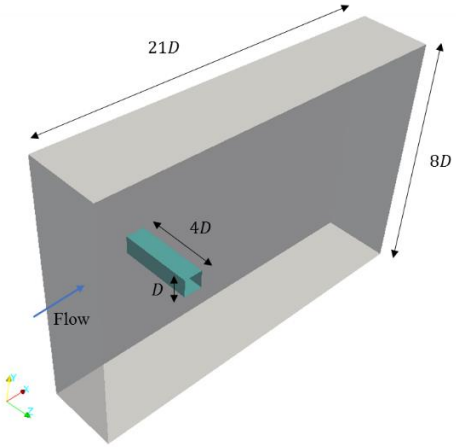

Figure 1 Computational domain and geometry of the square cylinder

Computational Details

Mesh – The computational grid used for the numerical simulations contains 830000 cells. The mesh refinement is applied in the wake regions, as illustrated in Figure 2. The near-wall flow region of the cylinder is meshed with 5 layers and the y^+ surface-averaged value is around 3.

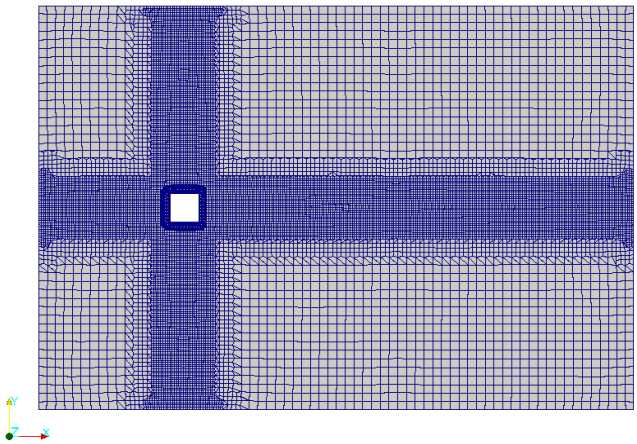

Figure 2 Coarse mesh view on the centre plane of the square cylinder

Boundary Conditions – The square cylinder surface is modelled as a non-slip wall while the upper and lower boundaries are applied a zero-friction condition. The side walls of the flow domain are treated as symmetry planes.

Solver - The transient simulation is carried out over 8 flow cycles - 1 flow cycle corresponds to the travelling time of the fluid from the inlet to the outlet of the computational domain. The flow fields are time-averaged over the last two flow cycles.

Results

Constant f_k - The second invariant of the velocity gradient, denoted by Q, is commonly used to identify the coherent structures of a transient turbulent flow. In fact, iso-surfaces of $Q > 0$ represent regions of high vorticity where the rotation rate is higher than the strain rate. The effect of the modelled-to-total scale ratio on these iso-surfaces is shown in Figure 3. Setting f_k to a reasonable constant value of 0.4 over the whole computational domain results in the appearance of new vortical structures that do not exist in the URANS simulation ($f_k = 1$). The difference in the resolution of turbulence scales between PANS and URANS clearly affects the mean axial velocity profile as illustrated in Figure 4. Superiority of PANS over URANS is quantitatively demonstrated in that plot.

Grid-based f_k- The different calculation methods of the f_k parameter are compared in Figure 5 and Figure 6. An overestimation of f_k can be observed for GB1 and GB2. As a result, most of the turbulence characteristics obtained with these methods are modelled. On the other hand, GB3 and GB4 show more resolved scales in the wake region and the corresponding velocity profiles are closer to the experiment. The mean drag coefficient and the Strouhal number for the different cases are all reported in Table 3.

Convection scheme – The usage of a blended central differences-upwind convection scheme for the momentum equation sometimes helps stabilize a non-converging transient solution. Nevertheless for a PANS simulation, the contribution of the first-order scheme can have an inhibiting effect on the resolution of critical turbulence scales. Figure 7 and Figure 8 show that despite low f_k values in the wake and apparent multi-scale vortices, the actual PANS solution is very similar to the URANS one.

Unresolved turbulent Prandtl numbers – The zero and maximum transport models are compared in Figure 9 and Figure 10. The difference in the spatial distribution of f_k can be observed between the two cases. The zero transport model seems to be more diffusive as it produces lower f_k values in the detached flow regions. This is probably due to a higher diffusion coefficient, resulting from a division by f_k (ranging from 0 to 1), in the equation of the unresolved turbulent kinetic energy. Despite this difference, the overall flow structures and the mean axial velocity profile are similar for both transport models.

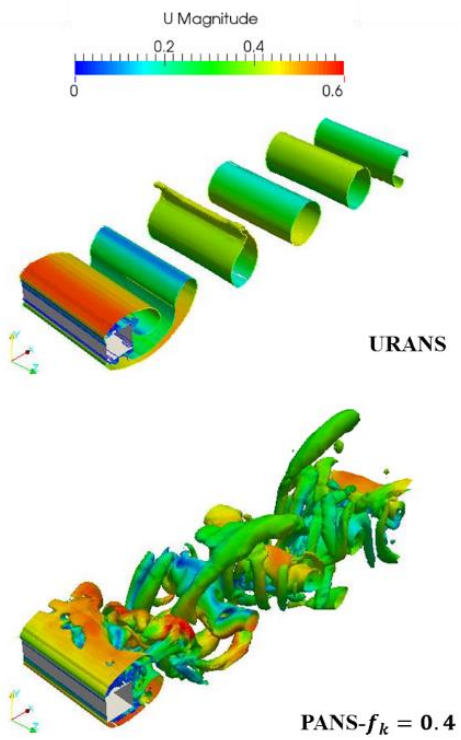

Figure 3 Coarse mesh. Instantaneous iso-surfaces of the Q criterion ($Q = 0.01\ s^{-1}$)

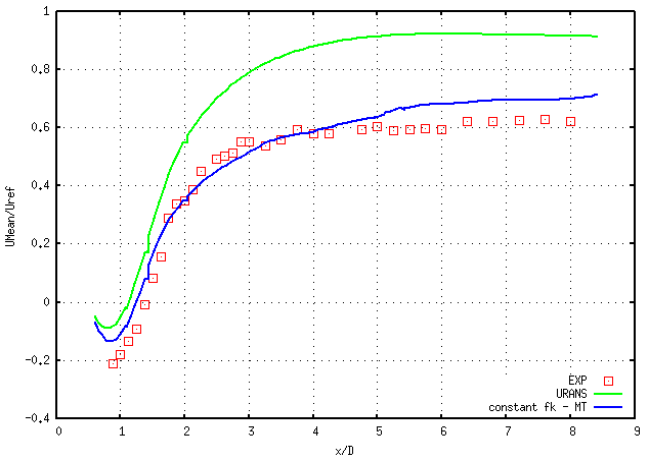

Figure 4 Coarse mesh. Mean axial velocity profile - Experiment (red symbol), URANS (green), $f_k = 0.4$ (blue)

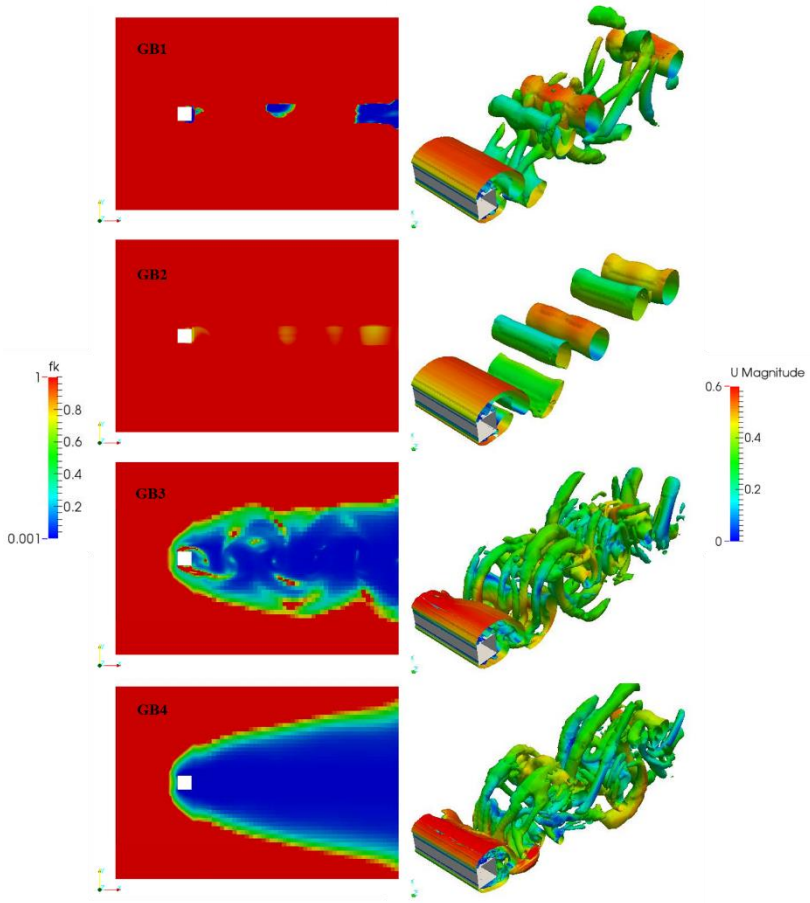

Figure 5 Coarse mesh. Representation of f_k in the symmetry plane of the cylinder (left), instantaneous iso-surfaces of $Q = 0.01\ s^{-1}$ (right) for GB1, GB2, GB3 and GB4 (from top to bottom)

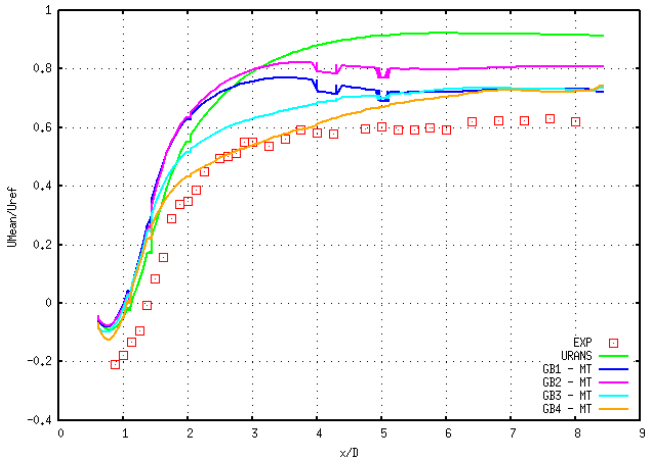

Figure 6 Coarse mesh. Mean axial velocity profile - Experiment (red symbol), URANS (green), GB1 (dark blue), GB2 (pink), GB3 (light blue), GB4 (orange)

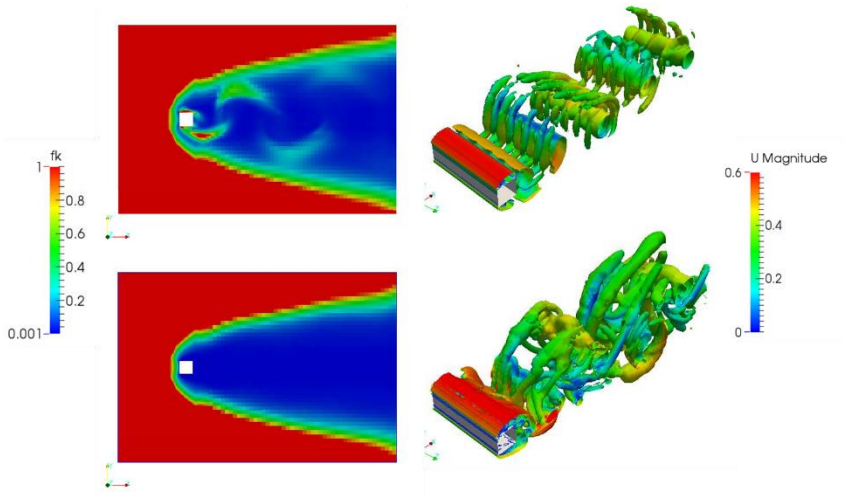

Figure 7 Coarse Mesh. PANS GB4 –Blended central differences (0.4) – upwind scheme (top), Second-order upwind scheme (bottom)

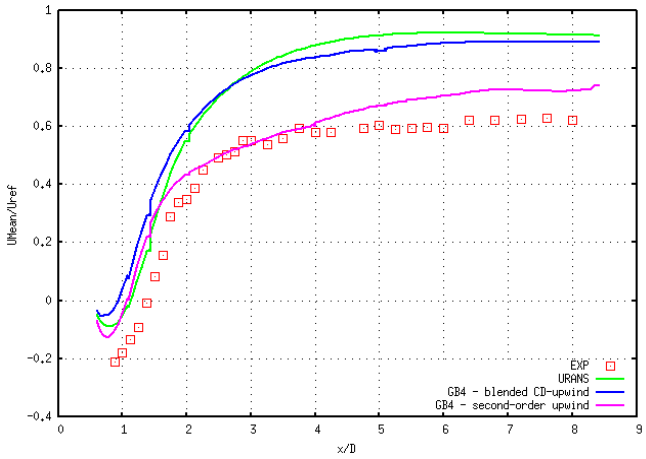

Figure 8 Coarse Mesh. Mean axial velocity profile - Experiment (red symbol), URANS (green), GB4 second-order upwind (pink), GB4 Blended central differences (0.4) – upwind scheme (blue)

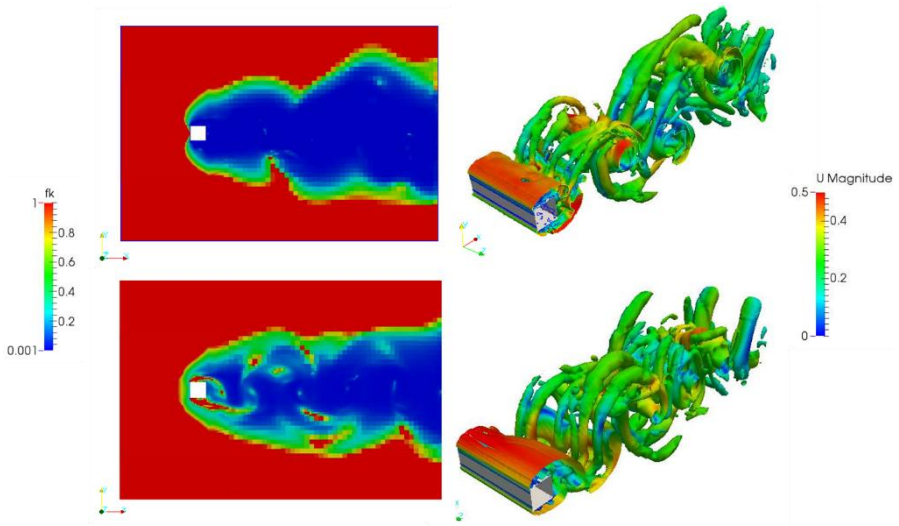

Figure 9 Coarse Mesh. PANS GB3 – Zero Transport Model (top), Maximum Transport Model (bottom)

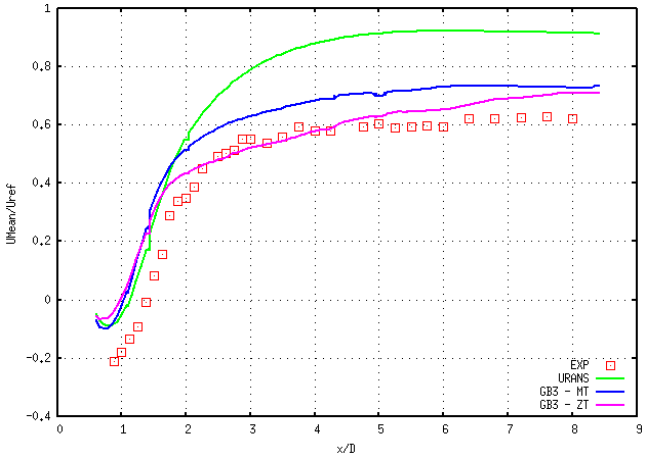

Figure 10 Coarse Mesh. Mean axial velocity profile - Experiment (red square), URANS (green), GB3 Zero Transport Model (pink), GB3 Maximum Transport Model (blue)

	C_D	C_D − error (%)	Str	Str − error (%)
Exp.	2.1	-	0.132	-
URANS	2.01	-4.5	0.144	8.8
Constant f_k	2.09	-0.5	0.123	-6.5
GB1	2.08	-1.1	0.141	7
GB2	2.08	-1.2	0.154	16.7
GB3	2.09	-0.4	0.127	-3.3
GB4	2.09	-0.5	0.124	-6

Table 3 Coarse mesh. Mean drag and Strouhal number for the different cases

3.2.2. Flow past a surface-mounted cube

It is important to assess the accuracy of the PANS model in simple turbulent wall-bounded flows before using it in the context of ground vehicles aerodynamics. The surface-mounted cube is a good test case for that as it involves unsteady separated flow regions and wake reattachment on the wall. A detailed description of the vortex structures as well as measurements of the flow statistics can be found in the experimental study of Martinuzzi and Tropea [11].

Case Description

The Reynolds number of the flow, based on the cube height H, is 80000. This gives a reference bulk velocity of $48\,m.s^{-1}$, if H is set to $0.025\,m$. The geometric dimensions of the computational domain, proportional to H, are represented in Figure 11. The velocity profile at the channel inlet is interpolated from the experimental data to simulate a fully developed turbulent upstream flow. The vortex structures and the velocity profiles in the symmetry plane of the cube will be compared to the experiment.

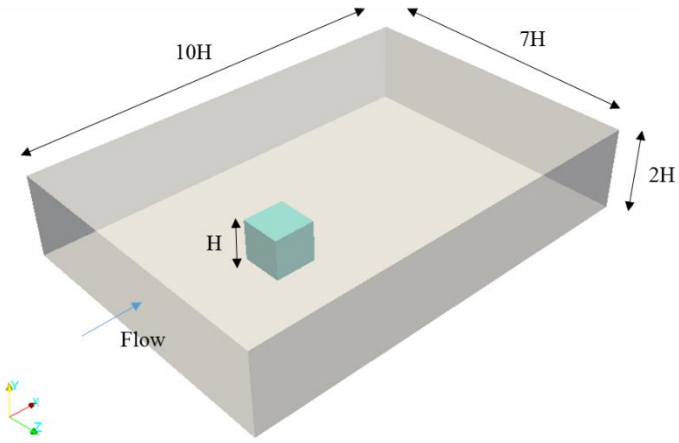

Figure 11 Computational domain and geometry of the surface-mounted cube

Computational Details

Mesh – In order to capture most of the flow details, the wake region of the cube is refined twice with respect to the coarsest mesh regions, as shown in Figure 12. The number of layers is set to 5 on all the non-slip walls and the y^+ surface-averaged value is equal to 10. The total cell count of the computational grid is 1800000.

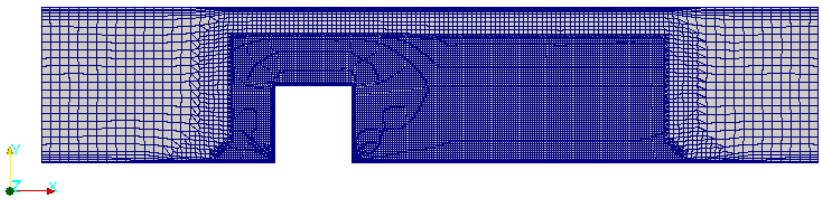

Figure 12 Mesh view in the symmetry plane of the surface-mounted cube

Boundary Conditions – The cube surface as well as the channel upper and lower boundaries are modelled as non-slip walls. The side boundaries of the flow domain are set to symmetry planes.

Solver – The total number of iterations for the transient simulation corresponds to 10 flow cycles - 1 flow cycle is defined as the travelling time of the fluid from the inlet to the outlet of the channel. The flow fields are time-averaged over the last two flow cycles.

Results

Flow topology – Iso-surfaces of the second invariant of the velocity gradient Q are compared between URANS and PANS-GB4 in Figure 14. In addition to the upstream trumpet vortex on the floor, which is present in both simulations, the PANS solution features richer multi-scale turbulent structures in the wake region of the cube.

Velocity field – Figure 15 shows the time-averaged streamlines in the symmetry plane of the flow. The experimental value of the downstream primary recirculation length is estimated at $1.612H$ [11]. In the PANS case, that length is better predicted as it is equal to $1.6H$ against $2H$ for URANS. Figure 17 shows the mean axial velocity profiles in the wall normal direction at five different locations of the flow represented in Figure 16. Overall, the PANS and URANS solutions are very similar except at $x/H = 4$ for which the PANS profile is closer the experiment.

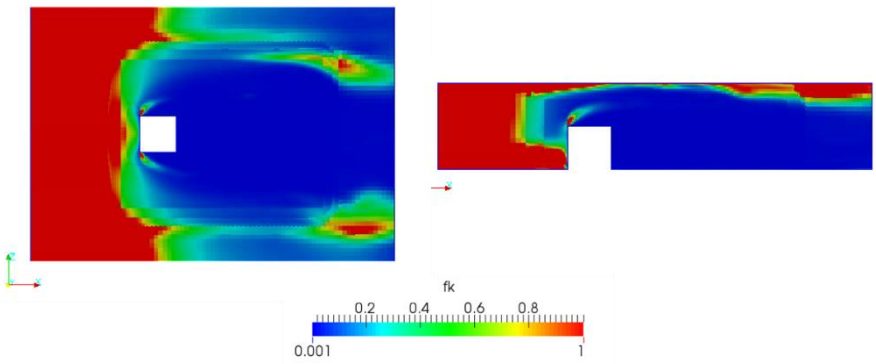

Figure 13 f_k field in the symmetry planes of the cube – $y = 0.5H$ (left), $z = 0H$ (right)

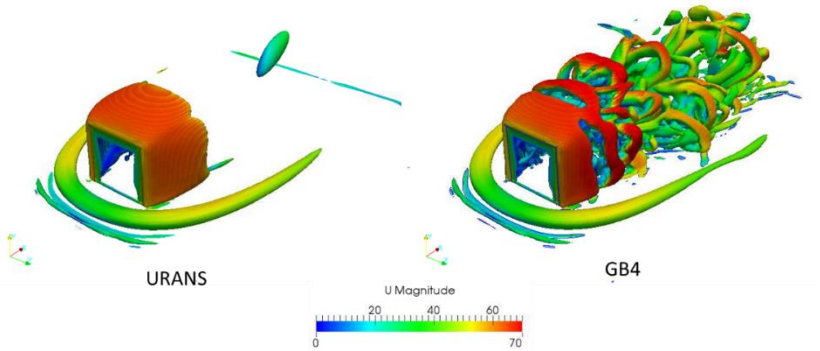

Figure 14 Surface-mounted cube. Iso-surfaces of the Q criterion

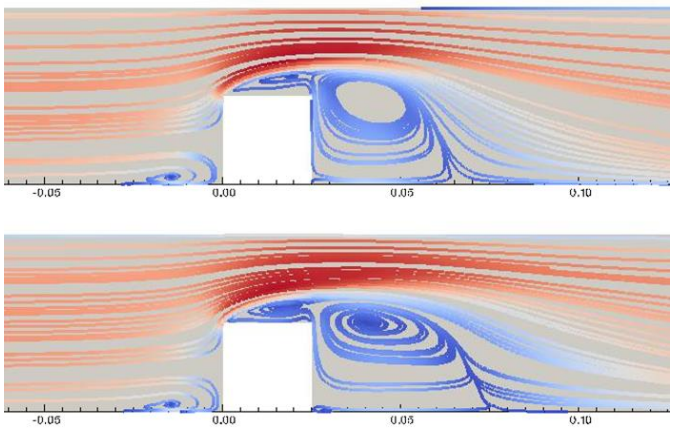

Figure 15 Streamlines on the symmetry plane of the cube – PANS GB4 (top), URANS (bottom)

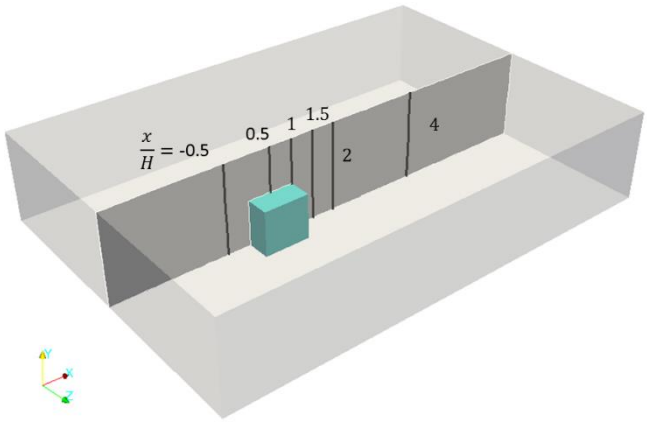

Figure 16 Locations of experimental probes in the symmetry plane of the surface-mounted cube

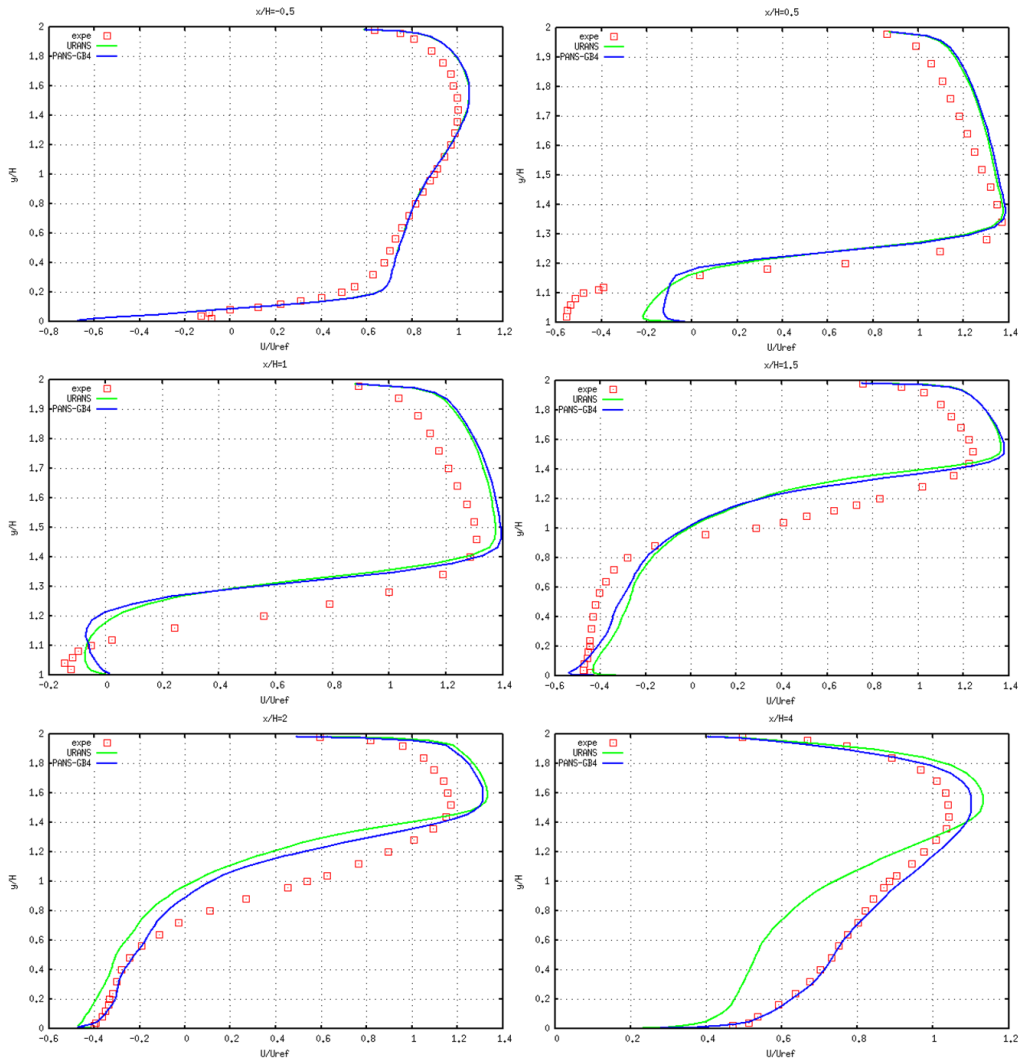

Figure 17 Mean axial velocity in the symmetry plane of the surface-mounted cube – Experiment (red symbols), PANS GB4 (blue), URANS (green)

3.3. Automotive External Aerodynamics

In this section, the PANS model is validated on a full-scale industrial case. The car model is of type hatchback. It is generally difficult to correctly predict the flow over this type of car by CFD methods. The flow in the wake of the car is very complicated and inherently unsteady. With the growing pressure on aerodynamic optimizations of road cars, the ability to quickly and accurately predict the aerodynamics is very important.

Case Description

The 1:1 detailed mock-up model is considered in the current validation study. The car model is displayed in Figure 18, the bulk dimensions of the car are approximately (3.8m × 1.7m × 1.6m). The computational domain is a rectangular numerical wind tunnel with dimensions (60m × 50m × 30m) displayed in Figure 18. At the inflow plane the flow velocity U_∞ = 38.89 m/s was specified. At the top plane, side planes and outlet plane the zero value of the relative pressure and zero gradient boundary conditions for all turbulent variables were applied. The

floor plane is divided into parts where no-slip and symmetry boundary conditions were applied. The distance between car centre and start of the no-slip condition was chosen so to reach the thickness of the boundary layer corresponding to wind tunnel measurement. The computational domain is sufficiently large to reduce influence of the computational wind tunnel boundaries on the flow around the vehicle.

The computational mesh created with iconHexMesh consists of 68 million cells. The resulting mesh is polyhedral (hex-dominant) with multiple regions of refinement around the car and its wake as can be seen in Figure 19. To properly refine mesh near the car surface two consecutive distance-based refinements are done as displayed in Figure 19. The whole car surface is covered by 4 prismatic layers resulting in the dimensionless wall distance $y^+ \sim 30$. The surface mesh is refined in areas of high curvature.

The numerical schemes and the solution procedure were described in Section 3.1. The GB2 method for the calculation of f_k was chosen for the industrial case. The time step was set to $\Delta t = 0.0001s$ in order to achieve a maximum CFL ($\sim U\Delta t/\Delta x$) under 5.

The same mesh, numerical schemes and solution procedure was used to predict the flow with URANS $\zeta - f$ model ($f_k = 1$). In both PANS and URANS cases 1.5s of flow was calculated.

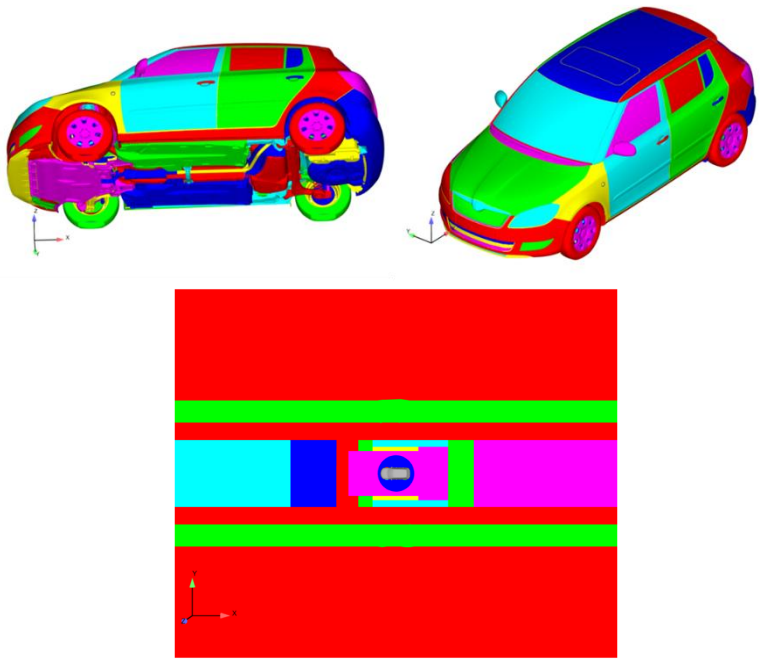

Figure 18 Car geometry and top view of the computational domain

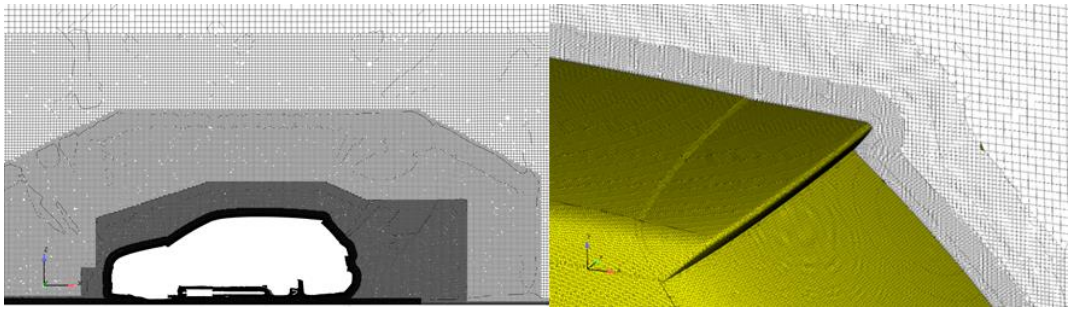

Figure 19 Mesh refinement around the car

Results

To evaluate the performance of the PANS model in the industrial external flow we must first check if the mesh resolution is sufficient to trigger the seamless transition between URANS and DNS. This depends on the parameter f_k, if $f_k < 1$ then the PANS results depart from URANS results. It can be seen from Figure 20 that the spatial resolution is fine enough to differ substantially from the URANS limit. The discontinuities in the f_k field are results of mesh refinement. It can be observed that the mesh resolution is not sufficient in some areas of the wake, especially in the far wake and in the areas with Helmholtz-Kelvin instability. To show capability of PANS modelling to predict strongly separated flow in the external car aerodynamic, we compare PANS results to URANS $\zeta - f$ model results. The overall solution time and HPC resources are the same between URANS and PANS.

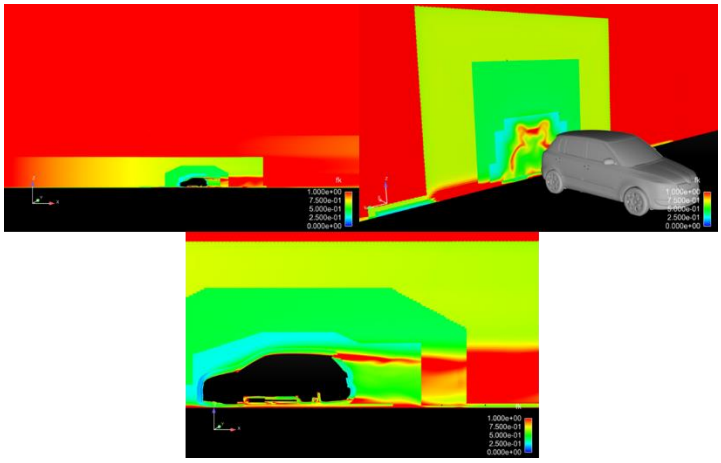

Figure 20 Unresolved-to-total ratio of the turbulent kinetic energy f_k instantaneous value

The vortex structure within the wake region and around the car is visualized by Q-criterion ($Q = 1000s^{-2}$) representing basically the second invariant of the velocity gradient tensor, see Figure 21. The predicted vortex structure is richer with the PANS model in the wake area and also in wakes of the wheels and mirrors. The structure of A-pillar vortex is also finer than with URANS. Figure 22 displays the complicated structure of the wake behind the car.

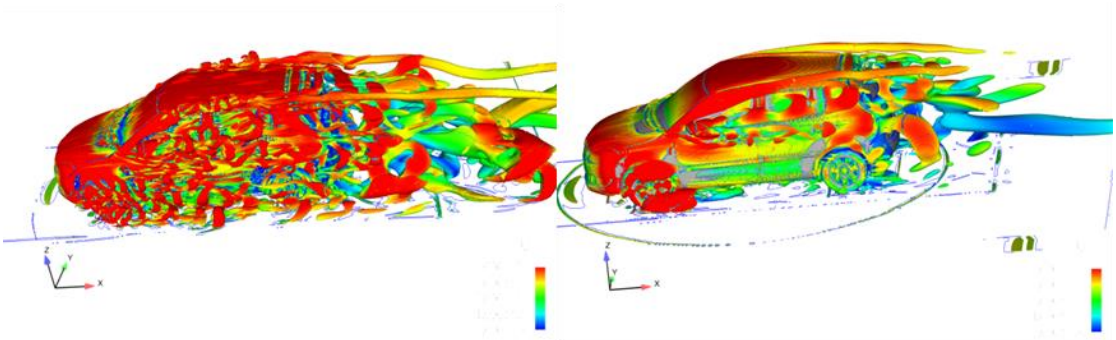

Figure 21 Flow field structures predicted by PANS (left) and URANS (right), visualized by the Q-criterion ($Q = 1000s^{-2}$) and coloured by velocity magnitude

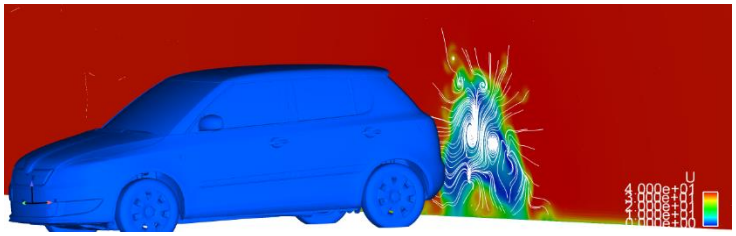

Figure 22 Instantaneous streamline pattern behind the car coloured by magnitude of instantaneous velocity

The CFD results are compared to experimental results. The flow around the car was experimentally examined in the VW wind tunnel. To have more information about the flow field the pressure strips measurement method was used, see Figure 25. Detailed view on the pressure strip is displayed in

Figure 23. This tool uses multiple connected pressure probes, details about the tool are described in [13]. The measured car was equipped with 24 pressure strips and each strip contains 24 pressure sensors; the distance between the probes is 1cm. The post-processing tool also described in [13] was used to compare pressure coefficient Cp on different parts of the car between wind tunnel experiment and CFD, see Figure 25, Figure 26, Figure 28 and Figure 29. We compare value of C_p and also pressure gradients on some parts of the car. The analysis of the pressure stripes shows very similar behaviour of the models in the front of the car; see Figure 25 and Figure 28. Also the comparison to experimental value of $C_p$is very good.

Differences between the models can be found on the back of the car, see Figure 27 and Figure 26. The PANS results are closer to experimental values of $C_p$on the rear bumper than the URANS results, see Figure 26. Larger discrepancies between the experimental values and the CFD result can be found on the fifth door; see Figure 27. This difference is reduced in PANS results. This discrepancy is possibly a result of a difference between real wind tunnel geometry and the numerical domain where some important effects (horizontal buoyancy, effect of nozzle and collector shape) are omitted. This issue will be addressed in the future by using more realistic wind tunnel geometry and also by using wind tunnel correction on the experimental results.

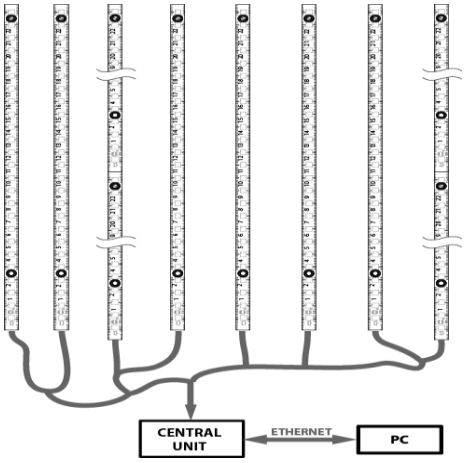

Figure 23 Pressure strips

Both methods resulted in similar averaged values of a drag coefficients C_d, both methods overpredicted the values measured in the wind tunnel, the delta between experiment and CFD was by 10% smaller with PANS than with URANS. Very similar improvement was observed also for the lift coefficient C_l.

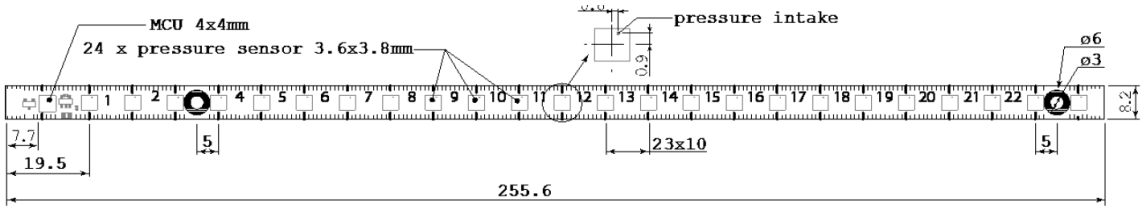

Figure 24 Pressure strip

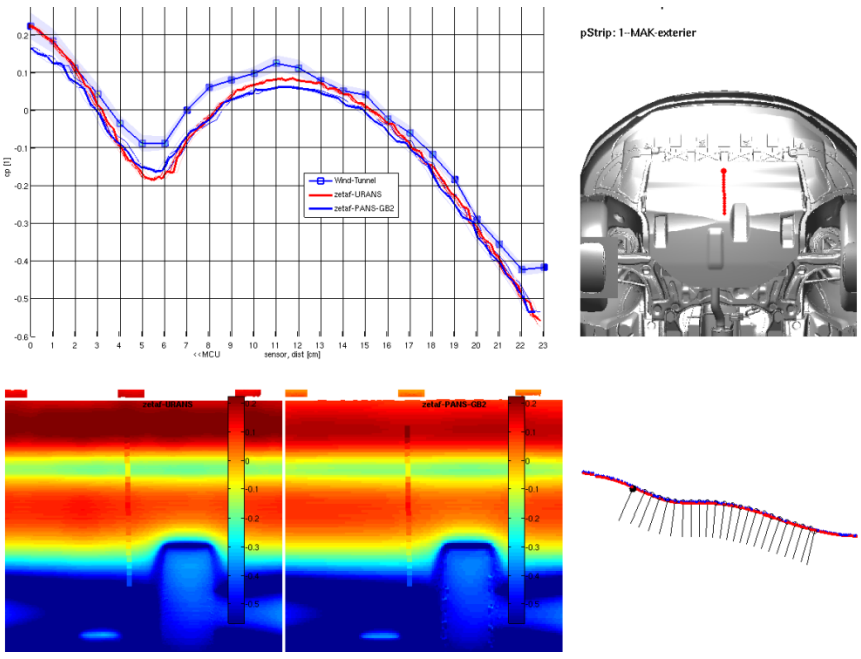

Figure 25 Pressure strip on engine cover

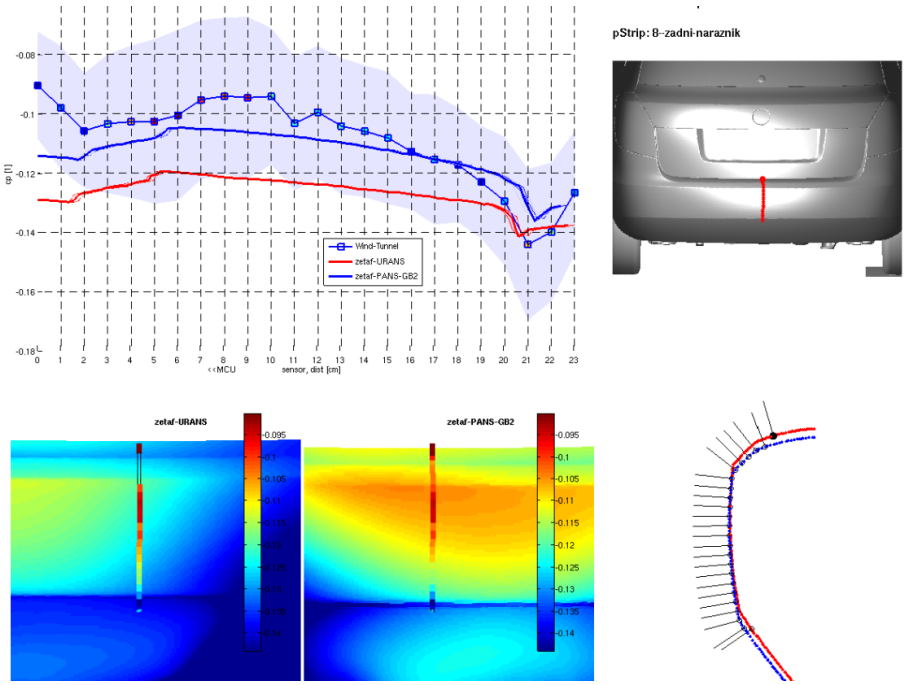

Figure 26 Pressure strip on rear bumper

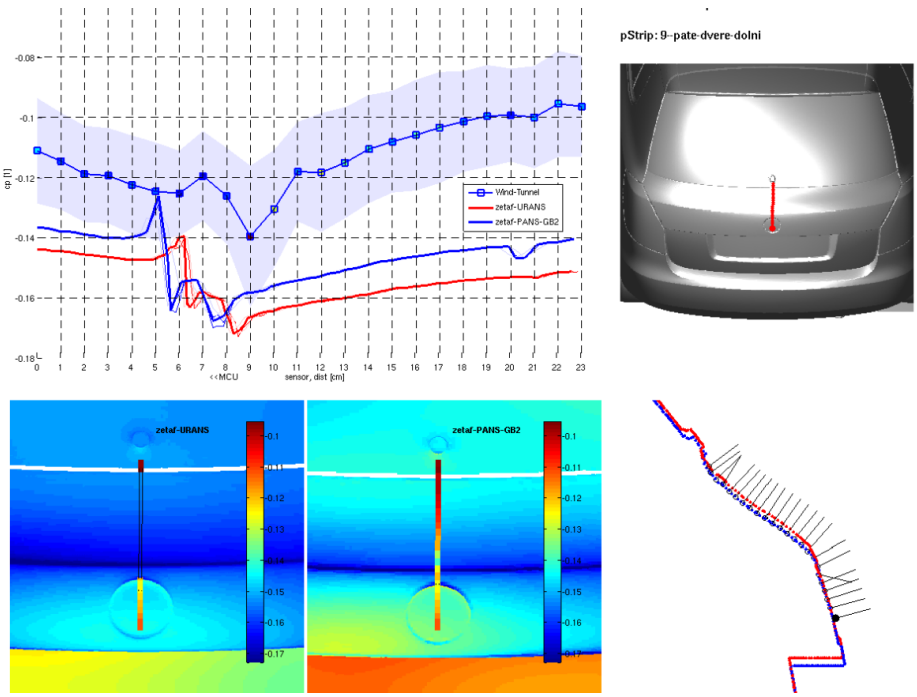

Figure 27 Pressure strip on fifth door

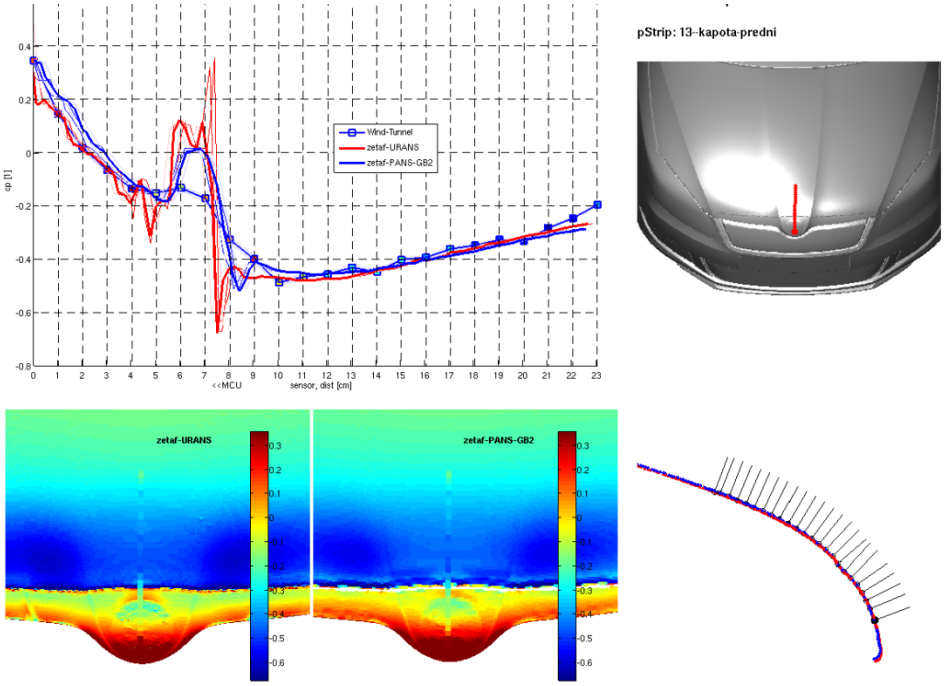

Figure 28 Pressure strip in the front of the car

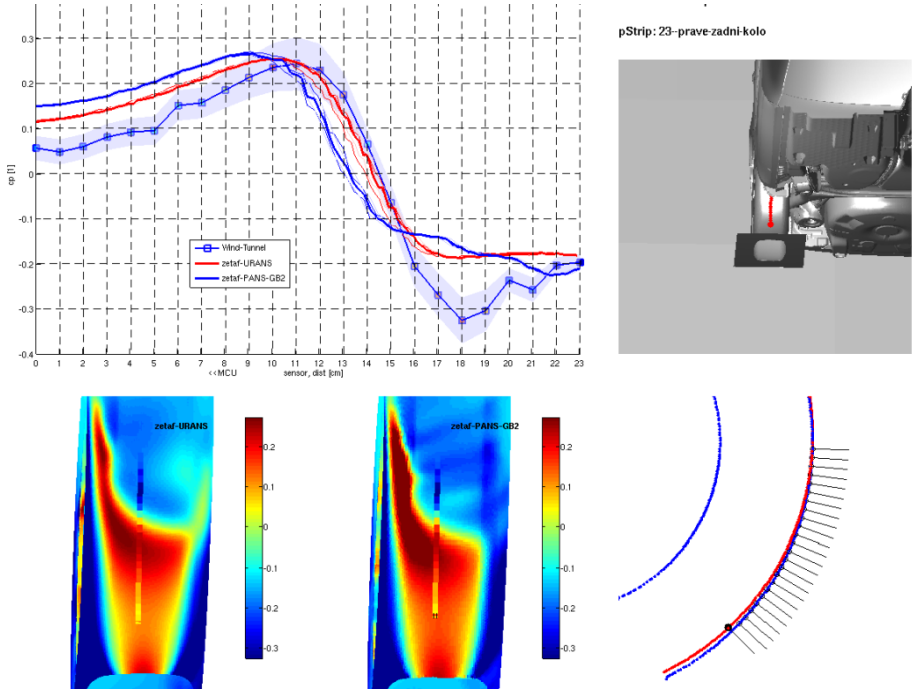

Figure 29 Pressure strip on rear right wheel

4. Summary

A PANS $\zeta - f$ turbulence modelling framework was implemented in the iconCFD® simulation toolkit. Four different methods for the calculation of f_k were analysed on three cases: the square cylinder, the surface-mounted cube and a SKODA vehicle model. In all cases,

the PANS implementation has showed both in the richness of the turbulent content as well as in the improved accuracy of the results. Further investigation needs to be done in the stability issues of the GB4 method which provides the best accuracy. For external aerodynamics simulations, the authors currently recommend the use of the GB2 method which provides a good compromise between accuracy and stability.

5. Acknowledgements

The work presented here was carried out in collaboration with ŠKODA who kindly accepted to provide validation materials for testing the PANS $\zeta - f$ model. The authors of this paper are grateful for this greatly acknowledged contribution.

REFERENCES

1. Jochen Frohlic, D. v. (2008). Hybrid LES/RANS methods for the simulation of turbulent flows. Progress in Aerospace Sciences 44, 349-377.
2. Girimaji S. S. (2006). Partially-Averaged Navier-Stokes Model for Turbulence: A Reynolds-Averaged Navier-Stokes to Direct Numerical Simulation Bridging Method. Journal of Applied Mechanics, 413-421.
3. Girimaji S. S. (2005). Partially-averaged Navier Stokes Model for Turbulence: Implementation and Validation. AIAA 2005-0502, 1-14.
4. Branislav Basara et al. (2011), Near-Wall Formulation of the Partially Averaged Navier-Stokes Turbulence Model. AIAA Vol. 49, No. 12, 2627-2635.
5. M. Germano (1992), Turbulence: the filtering approach. Journal of Fluid Mechanics Vol. 238, 325-336.
6. K. Hanjalic et al. (2004). A robust near-wall elliptic-relaxation eddy-viscosity turbulence model for CFD. International Journal of Heat and Fluid Flow 25, 1047-1051.
7. M. Popovac, K. Hanjalic (2007). Compound Wall Treatment for RANS Computation of Complex Turbulent Flows and Heat Transfer. Flow Turbulence Combust 78, 177-202.
8. Lyn D.A, Rodi W. (1994). The flapping shear layer formed by flow separation from the forward corner of a square cylinder. Journal of Fluid Mechanics, 267-353.
9. Lyn D.A et al. (1994). A laser-Doppler velocimetry study of ensemble-averaged characteristics of the turbulent near wake of a square cylinder. Rept. SFB 210 /E/100.
10. Rodi W. (1997). Comparisons of LES and RANS calculations of the flow around bluff bodies. J. Wind Eng. Ind. Aerodyn. 69-71, 55-75.
11. Martinuzzi R., Tropea C. (1993). The Flow Around Surface-Mounted, Prismatic Obstacles Placed in a Fully Developed Channel Flow. Journal of Fluids Engineering, Vol. 115, 85-92.
12. http://cfd.mace.manchester.ac.uk/ercoftac/
13. Filipský J., Polická P., Čížek J. (2015). Multipoint Pressure Strip Measurement for Advanced CFD Validation. 10th FKFS-Conference, Progress in vehicle Aerodynamics and Thermal Management.